Structural insight into substrate specificity of phosphodiesterase 10

Huanchen Wang*, Yudong Liu*, Jing Hou*†, Meiyan Zheng*, Howard Robinson‡, and Hengming Ke*§

*Department of Biochemistry and Biophysics and Lineberger Comprehensive Cancer Center, University of North Carolina, Chapel Hill, NC 27599-7260; and ‡Department of Biology, Brookhaven National Laboratory, Upton, NY 11973-5000

Edited by Joseph A. Beavo, University of Washington School of Medicine, Seattle, WA, and approved February 20, 2007 (received for review January 11, 2007)

Phosphodiesterases (PDEs) hydrolyze the second messengers cAMP and cGMP. It remains unknown how individual PDE families selectively recognize cAMP and cGMP. This work reports structural studies on substrate specificity. The crystal structures of the catalytic domains of the D674A and D564N mutants of PDE10A2 in complex with cAMP and cGMP reveal that two substrates bind to the active site with the same *syn* configuration but different orientations and interactions. The products AMP and GMP bind PDE10A2 with the *anti* configuration and interact with both divalent metals, in contrast to no direct contact of the substrates. The structures suggest that the *syn* configurations of cAMP and cGMP are the genuine substrates for PDE10 and the specificity is achieved through the different interactions and conformations of the substrates. The PDE10A2 structures also show that the conformation of the invariant glutamine is locked by two hydrogen bonds and is unlikely to switch for substrate recognition. Sequence alignment shows a potential pocket, in which variation of amino acids across PDE families defines the size and shape of the pocket and thus determines the substrate specificity.

crystal structure | cyclic nucleotides cAMP and cGMP

Cyclic nucleotide phosphodiesterases (PDEs) are enzymes hydrolyzing the second messengers adenosine and guanosine 3′,5′-cyclic monophosphates (cAMP and cGMP). The human genome encodes 21 PDE genes that are categorized into 11 families (1, 2). Selective inhibitors against individual PDE families have been developed as therapeutics for treatment of various human diseases (3–8). The best known examples are the PDE5 inhibitors sildenafil (Viagra), vardenafil (Levitra), and tadalafil (Cialis) that have been used for treatment of male erectile dysfunction (5). Sildenafil (Revatio) has also been approved for treatment of pulmonary hypertension (9).

PDE10 was independently identified by three groups in 1999 and shows a dual activity on hydrolysis of both cAMP and cGMP (10–12). PDE10 is highly expressed in brain striatum (13–16). Reduction of PDE10A mRNA and protein levels in striatum of transgenic mice implies a role of PDE10A in Huntington's disease (17, 18). Knockout mice experiments suggest that PDE10A is involved in regulating striatal output, possibly by reducing the sensitivity of medium spiny neurons to glutamatergic excitation (19). The PDE10 inhibitor papaverine is effective in improving executive function deficits associated with schizophrenia, and therefore inhibition of PDE10 may represent an approach to treatment of psychosis (20, 21).

PDE families contain a variable N-terminal regulatory domain and a conserved C-terminal catalytic domain. Individual PDE families show different substrate preferences. Crystal structures have been reported for the catalytic domains of seven PDE families in the unliganded form or in complex with inhibitors or products: PDE1B, PDE2A, PDE3B, PDE4B/4D, PDE5A, PDE7A, and PDE9A (22–34). However, it remains a puzzle how the conserved catalytic pocket of the PDE families selectively recognizes cAMP and cGMP. On the basis of the crystal structures of PDE4-AMP and PDE5-GMP, a "glutamine switch" mechanism was proposed for the substrate specificity (31). However, this mechanism is challenged by the mutagenesis experiments, in which the Q817A mutation in PDE5A1 did not significantly impact cAMP binding (35).

We have performed a systematic structural study on the substrate specificity of PDE10A2. Reported here are eight crystal structures of the catalytic domains of the wild-type PDE10A2 in the unliganded state or complex with products AMP and GMP, the D674A mutant and its complexes with substrates cAMP and cGMP, and the D564N mutant and its complex with cAMP. These structures reveal the conformation and interactions of substrates cAMP and cGMP in PDE10A2 and suggest a pocket that may determine the substrate specificity.

Results

Kinetic Properties of the Catalytic Domain of PDE10A2. The catalytic domain of PDE10A2 (449–789) has a K_m and k_{cat} of 56 nM and 0.33 s^{-1} for cAMP and 4.4 μM and 1.2 s^{-1} for cGMP. The k_{cat}/K_m values are 5.9 and 0.27 $s^{-1}\cdot\mu M^{-1}$, respectively, for cAMP and cGMP, and the specificity constant $(k_{cat}/K_m)^{cAMP}/(k_{cat}/K_m)^{cGMP}$ is 22. These numbers suggest a dual substrate specificity of PDE10A2, although the enzyme is more effective toward cAMP. The V_{max} values of our PDE10A2 catalytic domain are 507 nmol/min per mg for cAMP and 1,860 nmol/min per mg for cGMP and are comparable with those for the full-length PDE10A1 (10). There are two divalent metal ions at the active site of wild-type PDE10A2. The first ion coordinates with His^{529}, His^{563}, Asp^{564}, and Asp^{674}, and two waters, and has the same interactions as zinc in PDE4 (23). The second metal coordinates with Asp^{564} and five water molecules.

The D674A mutant lost at least 4 orders of magnitude in the catalytic activity, as shown by an assay in which no activity was observed at 40 μg/ml D674A mutant, compared with only 5 ng/ml wild-type enzyme required for a normal assay. A consequence of the D674A mutation is loss of zinc ion, as confirmed by no electron density for the zinc site in the structures of unliganded D674A, D674A-cAMP, and D674A-cGMP. This observation implies that zinc is not critical for assembly of the PDE subdomains (23) but is essential for the catalysis. The

Author contributions: H.W. and H.K. designed research; H.W., J.H., and M.Z. performed research; Y.L. and H.R. analyzed data; and H.K. wrote the paper.

The authors declare no conflict of interest.

This article is a PNAS Direct Submission.

Abbreviations: PDE, cyclic nucleotide phosphodiesterase; S-pocket, substrate specificity pocket.

Data deposition: The atomic coordinates and structure factors have been deposited in the Protein Data Bank, www.pdb.org (PDB ID codes 2OUN, 2OUP, 2OUQ, 2OUR, 2OUS, 2OUU, 2OUV, and 2OUY).

†Present address: School of Pharmaceutical Sciences, Sun Yat-sen University, Guangzhou 510080, China.

§To whom correspondence should be addressed. E-mail: hke@med.unc.edu.

This article contains supporting information online at www.pnas.org/cgi/content/full/0700279104/DC1.

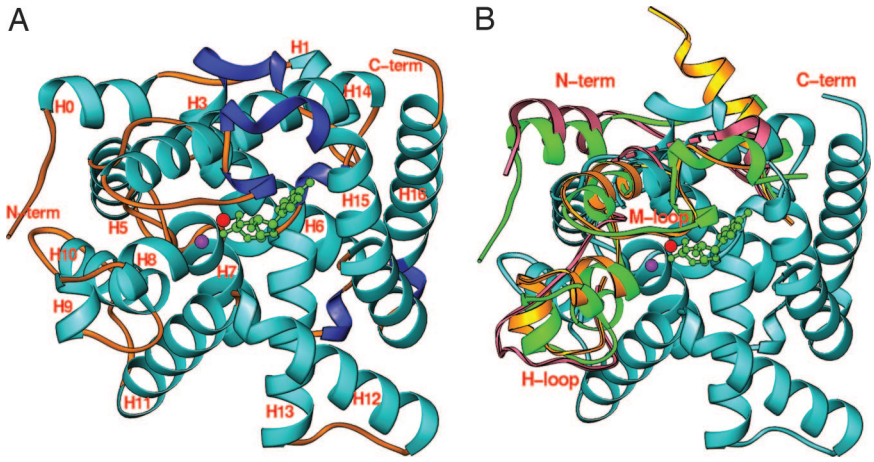

Fig. 1. Structures of the catalytic domain of PDE10A2. (*A*) Ribbon diagram. Divalent metals zinc and magnesium are shown in red and purple. Green balls–sticks represent cAMP. (*B*) Superposition of PDE10 (green ribbons) over PDE4 (gold) and PDE5 (salmon). Cyan ribbons represent comparable regions among three structures.

D564N mutant has the catalytic activity <1/1,000 of the wild-type PDE10A2, although both divalent metals are found in the D564N structures.

Architecture of PDE10 Structures. Although the PDE10A2 catalytic domain with residues 449–789 was used in the crystallization, only 449–770 can be traced unambiguously in the maps. The C-terminal residues 771–789 in all of the crystals and residues 571–586 of molecule B in the structures of PDE10A-GMP, D674A-cAMP, D674A-cGMP, and D564N-cAMP cannot be traced. Three residues from the expression vector, Ser^{446}, His^{447}, and Met^{448}, have clear electron density and are included in the structures.

The catalytic domain of PDE10A2 contains 15 α-helices and no β-strands (Fig. 1). The topological folding of PDE10A2 is the same as those of known structures of seven PDE families. The superposition of the PDE10A2 catalytic domain over the cAMP-specific PDE4D2 and the cGMP-specific PDE5A1 yielded rmsd values of 1.2 Å for the backbone atoms of 291 comparable PDE4D2 residues and 1.5 Å for 270 comparable PDE5A1 residues, indicating the overall similarity. The main difference between PDE10A2 and PDE4D2 occurs at the N terminus, in which H1 in PDE4D2 becomes a coil in PDE10A2 and H2 in PDE4D2 corresponds to a 3_{10} helix. The short helix H4 in PDE4 is missing in PDE10A2, probably resulting from the absence of 2 aa. However, PDE10A2 contains an extra helix at the N terminus, which occupies a location similar to that in PDE5A1 with a positional difference ≈3 Å. The H-loop of PDE10A2 (residues 571–592) contains two short α-helices and is comparable with that of PDE4D2 but not PDE5A1, in which the H-loop has variable conformations (34).

All eight crystal structures have the same space group with similar cell dimensions (Table 1) and contain two catalytic domains in their asymmetric units, which are related by a rotation axis of ≈100°. Because this angle differs from a twofold axis, the association of two PDE10A2 molecules appears to be crystallographic packing but is not biologically relevant. Superposition of molecules A over B yielded rmsd values of 1.4–1.6 Å for the eight structures, suggesting conformational changes of some loops. Indeed, residues 689–718 of the M-loop shift their C$^{\alpha}$ atoms as much as 7.5 Å, whereas other portions of the molecule remain comparable. The movements appear to be forced by the crystal lattice packing, as shown by the fact that the transposition of molecule A to B results in a clash with symmetry-related molecules.

No Significant Conformational Changes on Mutation or Substrate Binding. Structural superposition of the D564N and D674A mutants over the unliganded PDE10A2 yielded rmsd values of 0.10 and 0.12 Å for the C$^{\alpha}$ atoms of molecule A, 0.18 and 0.17 Å for molecule B, indicating no conformational changes on the mutations. The binding of cAMP, cGMP, or GMP caused 2.5–4.7% shrinking in the crystallographic *a* axis of D674A-cAMP, D564N-cAMP, D674A-cGMP, and PDE10A2-GMP (Table 1) and disorder of the H-loop residues 671–685 in molecule B of these structures. However, superposition of the unliganded PDE10A2 structure over PDE10A2-AMP, PDE10A2-GMP, D674A-cAMP, D564N-cAMP, and D674A-cGMP yielded rmsd values of 0.13, 0.24, 0.33, 0.28, and 0.29 for molecule A, and 0.16, 0.28, 0.72, 0.53, and 0.80 for molecule B, implying overall conformational similarity. A careful examination showed that residues Lys^{705}–Ile^{708} of the M-loop shift as much as 4 times the average rmsd in the five substrate–product complex structures. These changes appear to be the consequence of lattice contacts promoted by the hydrogen bond of cAMP/cGMP with the carbonyl oxygen of Leu^{706} of a symmetry-related molecule. In addition, the N-terminal residues 462–470 and 480–482 in molecule A of D674A-cGMP showed C$^{\alpha}$ positional changes 2–4 times the average difference because of the additional binding of cGMP to the N terminus. The only biologically significant change is the reorientation of the side chain of Leu^{635} of molecule A in the structures of D674A-cAMP and D564N-cAMP to avoid clashing with the ribose of cAMP.

Different Binding of Substrates cAMP and cGMP. Substrates cAMP and cGMP bind only at the active site of molecule A but not B of PDE10A2 (Fig. 2). The failure of substrate binding to B is probably because of the movement of both helix H14 and the M-loop into the active site [supporting information (SI) Fig. 5]. For example, Ile^{692} of H14 is located ≈4 Å to Phe^{729} in molecule B and thus blocks the interactions of the purines of cAMP and cGMP with Phe^{729} and Gln^{726}. The cAMP binding in the D674A-cAMP and D564N-cAMP structures is the same. The adenine of cAMP is sandwiched by Phe^{729} on one side and Ile^{692} and Phe^{696} on another side. N6 and N7 of adenine of cAMP form hydrogen bonds with OE1 and NE2 of Gln^{726}, respectively. The cyclic phosphate group of cAMP forms one hydrogen bond with His^{525} and three with water molecules. The ribose O5′ of cAMP hydrogen-bonds with a water molecule. O2′ forms two hydrogen bonds with a water molecule and the carbonyl oxygen of Leu^{706} from symmetry-related molecule B. In addition, cAMP interacts through van der Waals forces with residues Tyr^{524}, Leu^{635}, Leu^{675}, Val^{678}, Phe^{696}, and Met^{713} but does not directly contact the divalent metals. Substrate cAMP has a *syn* configuration and a 3′ *endo* ribose.

Three molecules of cGMP bind to the PDE10A2 catalytic

Table 1. Statistics on diffraction data and structure refinement

Data	10A native	10A-AMP	10A-GMP	D674A	D674A-cAMP	D674A-cGMP	D564N	D564N-cAMP
Space group	$P2_12_12_1$	$P2_12_12_1$	$P2_12_12_1$	$P2_12_12_1$	$P2_12_12_1$	$P2_12_12_1$	$P2_12_12_1$	$P2_12_12_1$
a, Å	51.1,	51.4	49.8	51.4	49.3	48.7	51.4	49.4
b, Å	82.0	82.0	81.9	82.0	82.3	82.0	82.2	82.3
c, Å	155.4	155.5	156.7	155.4	153.2	154.0	155.2	155.9
Resolution, Å	1.56	1.56	1.90	1.45	1.45	1.52	1.56	1.90
Reflections	85,847	87,893	48,795	110,590	101,420	95,665	91,666	47,078
Redundant	12.0	10.2	6.7	10.1	5.8	9.6	7.4	10.0
Complete, %	91.6 (58.5)*	93.3 (62.1)	94.8 (67.4)	94.4 (71.6)	90.9 (50.0)	99.9 (99.1)	97.0 (77.5)	92.3 (64.2)
Average I/σ	9.7 (2.2)	8.2 (2.0)	7.9 (2.0)	8.9 (2.1)	11.1 (2.2)	10.0 (2.5)	12.7 (3.3)	7.7 (2.1)
R_{merge}	0.067 (0.47)	0.094 (0.44)	0.071 (0.33)	0.077 (0.39)	0.073 (0.37)	0.082 (0.45)	0.064 (0.28)	0.078 (0.32)
Structure refinement								
R factor	0.197	0.200	0.213	0.209	0.218	0.204	0.209	0.217
R_{free}	0.223 (10)†	0.222 (10)	0.249 (10)	0.228 (10)	0.236 (10)	0.222 (10)	0.228 (10)	0.253 (10)
Reflections	81,787	83,987	47,053	101,832	96,206	92,068	89,422	45,261
rmsd for								
Bond, Å	0.0075	0.0064	0.0054	0.0066	0.0045	0.0063	0.0045	0.0058
Angle	1.3°	1.2°	1.2°	1.3°	1.3°	1.3°	1.1°	1.2°
Average *B* factor, Å^2								
Protein	22.9 (5,266)‡	19.5 (5,285)	27.1 (5,148)	20.6 (5,306)	19.6 (5,176)	19.7 (5,190)	19.9 (5,292)	26.9 (5,182)
Ligand		20.1 (23)	29.2 (24)		16.0 (22)	22.2 (69)		42.6 (22)
Waters	29.6 (425)‡	26.2 (399)	30.2 (322)	27.3 (425)	24.9 (437)	25.0 (366)	27.9 (458)	29.9 (320)
Zn	21.3 (2)‡	22.8 (2)	25.8 (2)				26.8 (2)	34.0 (2)
Mg	15.5 (2)‡	13.8 (2)	24.9 (2)	15.3 (2)	16.0 (2)	15.1 (2)	19.7 (2)	31.2 (2)

*The numbers in parentheses are for the highest resolution shell.
†The percentage of reflections is omitted for calculation of R_{free}.
‡The no. of atoms in the crystallographic asymmetric unit.

domain: one at the active site of molecule A and two in a pocket formed by the N-terminal residues of molecule A and symmetry-related molecules. The cGMP binding at the active site resembles that of cAMP in several aspects (Fig. 2), including the same *syn* configuration, shrinkage in *a* axis of the crystal, disorder of residues 571–586 in molecule B, and a hydrogen bond with the carbonyl oxygen of Leu^{706} from a symmetry-related molecule. However, significant differences between the binding of cAMP and cGMP are observed. The orientation of cGMP is flipped by ≈180° from that of cAMP, whereas their bases and phosphates occupy a similar location (Fig. 2). As result, the hydrogen bond of His^{525} with phosphate O2 of cAMP is swapped to O5′ of cGMP, and Gln^{726} forms only one hydrogen bond to N7 of cGMP.

An unexpected observation is that two molecules of cGMP bind to the N terminus of molecule A in D674A-cGMP. At this site, cGMP interacts with Ile^{450}–Ser^{453} of molecule A, symmetry-related residues of Leu^{547}, Leu^{654}–Leu^{656}, Gln^{743}–Pro^{747} of molecule A, and symmetry-related Leu^{466}–Lys^{470} of molecule B. The guanines of two cGMPs stack against one another and form three hydrogen bonds with Arg^{467} and Gln^{743} from symmetry-related molecules. The phosphate O2 forms two hydrogen bonds with Ser^{453} and Leu^{656}. Because this pocket does not exist in the structures in complex with cAMP, AMP, and GMP, it appears to be an artifact of the crystal packing. Nevertheless, the additional cGMP binding may lead to the positional shift of residues 462–471 and 480–483 of molecule B in D674A-cGMP, which is 2- to 4-fold the overall rmsd.

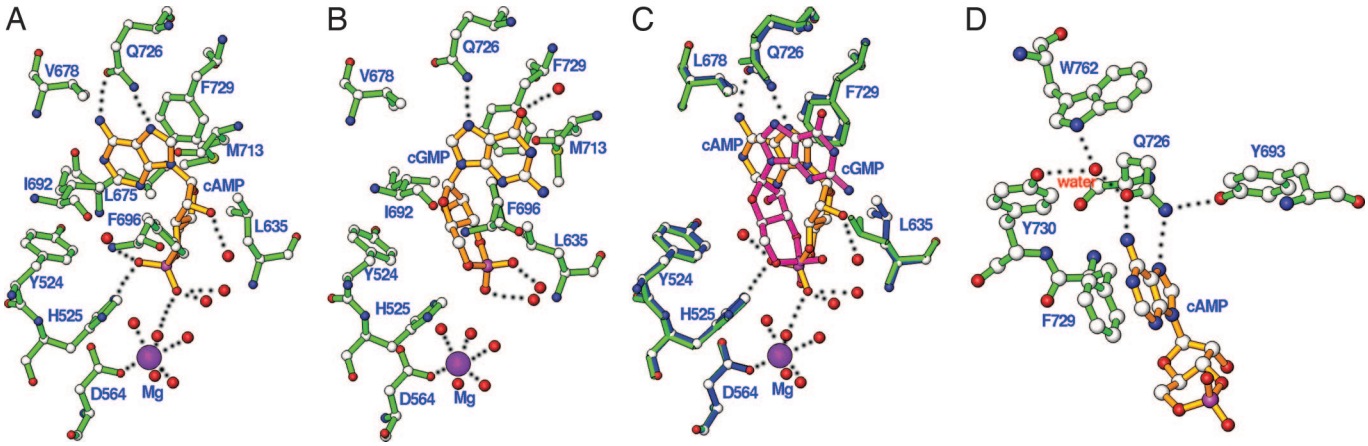

Fig. 2. Binding of cAMP and cGMP. (*A*) Interaction of cAMP (golden bonds) with PDE10A2 residues (green bonds) of the D674A mutant. The dotted lines represent hydrogen bonds. Small isolated red balls are water molecules. (*B*) Interaction of cGMP (gold) with D674A residues. (*C*) Superposition of cAMP (gold) over cGMP (pink). The residues from D674A-cAMP and D674A-cGMP are shown in blue and green, respectively. (*D*) Hydrogen bonds of Gln^{726} with Tyr^{693} and a water molecule bound to Trp^{762} and Tyr^{730}.

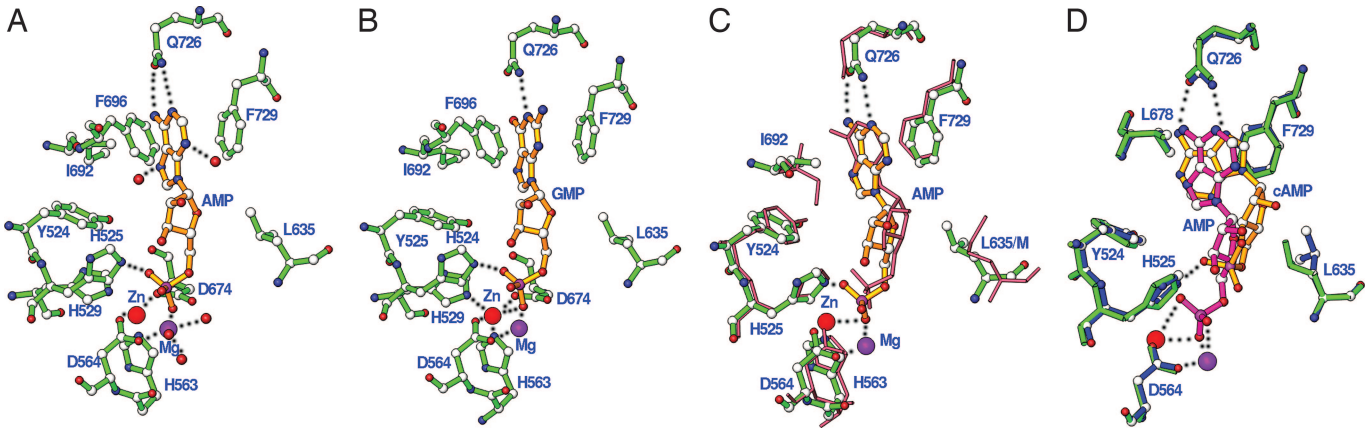

Fig. 3. Binding of products. (*A*) Interaction of AMP (gold) with PDE10A2 residues (green). (*B*) Interaction of GMP with PDE10A2 residues. (*C*) Superposition of PDE10A2-AMP over PDE4D2-AMP (salmon sticks) (27). (*D*) Superposition of AMP (pink) over cAMP (gold).

Products AMP and GMP Do Not Simulate Substrate Binding. The products AMP and GMP bind only to the active site of molecule A but not to molecule B. Both AMP and GMP have the same interactions and the same *anti* configuration and 3′ *endo* puckering (Fig. 3). The adenine of AMP and guanine of GMP are sandwiched by hydrophobic residues Phe^{729} on one side and Ile^{692} and Phe^{696} on another side. The adenine of AMP forms two hydrogen bonds with the side chain of Gln^{726} compared with only one between GMP and Gln^{726}. The interactions of AMP with PDE10A2 are the same as those in the structure of PDE4-AMP, in terms of hydrogen-bonding pattern, nucleotide conformation, and hydrophobic contact (Fig. 3*C*).

However, the contact pattern of the products AMP/GMP with the invariant glutamine is different from those of the substrates cAMP/cGMP although all of the ligands have the same stacking against Phe^{729} (Fig. 3*D*). The products have the *anti* configuration in contrast to *syn* of the substrates. Gln^{726} of PDE10A2 forms two hydrogen bonds with N1 and N6 of AMP and one with N1 of GMP. However, N6 and N7 of cAMP and N7 of cGMP are involved in hydrogen bonds with Gln^{726}. In addition, the phosphate groups of the products coordinate directly with both divalent metals and form hydrogen bonds with metal-bound residue Asp^{674} (Fig. 3). In comparison, the closest distance from the substrate atoms to the divalent metal ions is ≈4 Å, indicating no direct interaction.

Discussion

The Binding of cAMP and cGMP Simulates the Catalytic Process. Because the D674A and D564N mutants are basically inactive, it needs to be addressed whether the substrate binding in the crystal structures simulates the enzymatic process. The following observations suggest that the structural information is biologically relevant. First, the crystals of our PDE10A2 catalytic domain possess enzymatic activity, as shown by the fact that substrates cAMP and cGMP were hydrolyzed to AMP and GMP when the unmutated PDE10A2 crystals were soaked in the substrate solutions. Second, the wild-type PDE10A2 and the inactive mutants of D674A and D564N have almost identical conformations for the active-site residues, implying that substrate binding in the mutants simulates the biological process. Finally, the same conformation and interactions of cAMP in the mutant structures of D674A-cAMP and D564N-cAMP suggest that the metal ions do not directly impact the binding and conformation of the substrates. This hypothesis is supported by the fact that the closest distance of the substrate atoms to the metals is ≈4 Å in the D564N-cAMP structure. Therefore, we postulate that the substrate conformation and interaction in these crystal structures resemble those in the catalysis.

It has been reported that cAMP and cGMP exist in equilibrium between *syn* and *anti* configurations in solution, with *syn*:*anti* ratios of 30:70 and 95:5, respectively, for cAMP and cGMP (36). The $(F_o - F_c)$ and $(2F_o - F_c)$ maps, which were calculated from the structures before cAMP and cGMP were built in, show only the *syn* configuration of cAMP and cGMP bound to the active site of PDE10A2 (SI Fig. 6). Modeling of *anti* cAMP and cGMP into the pocket showed that the phosphate oxygen of the substrates clashes with two water molecules coordinated with zinc and magnesium, supporting that the *anti* conformers do not bind. Thus, the structures suggest that the *syn* conformer of cAMP and cGMP is the biological substrate for PDE10A2. However, it remains unknown which conformer of cAMP and cGMP is the genuine substrate for other PDE families. Early studies suggested that the preferable substrates are: *syn* cAMP and cGMP for PDE1 and PDE2, *anti* cAMP for PDE3 and PDE4, and *anti* cGMP for PDE3 and PDE5 (37, 38).

Because the substrates and products have different nucleotide configurations: *syn* for cAMP and cGMP, and *anti* for AMP and GMP, it would be interesting to know whether the enzyme takes an additional step to perform the *syn* to *anti* conversion during catalysis. To address this question, we carried out an activity assay in the presence of AMP and observed no significant inhibition by 5 mM AMP. On the basis of such poor binding of AMP, we hypothesize that the *syn* products leave the active site right after the catalysis, and the *syn* to *anti* conversion is not catalyzed by the enzyme but is an automatic process in solution. The occupancy of the *anti* AMP and GMP at the active site in the crystals may reflect the forced binding of the products at high concentration because they are predominant in solution (39). This argument is supported by the fact that only the *syn* configuration of 8-bromo-AMP was observed in the crystal when its *syn* configuration is predominant in solution (24, 39).

Implications for Substrate Specificity. The issue of the substrate specificity has not been extensively elucidated. The structures of PDE4D2-AMP, PDE4B2-AMP, and PDE5A1-GMP (24, 28, 31) show that the side chain of the invariant glutamine is fixed in opposite orientations in PDE4 and PDE5 and form two hydrogen bonds with products AMP and GMP. Because chemical formulas of AMP and GMP differ only in the phosphate portion from cAMP and cGMP, the conformation and interactions of nucleosides of the products have been assumed to simulate those of the substrates. This belief has led to a currently popular model, glutamine switch for the substrate specificity (31). In this mechanism, the glutamine is assumed to form two hydrogen bonds with cAMP but one with cGMP in cAMP-specific PDE families, and similarly cGMP-specific PDEs would have one hydrogen bond difference for the two

Table 2. Alignment of amino acids at the substrate-binding pocket

	678	685	689	692	693	713	725	726	729	730	762
PDE10A2	V	T	A	I	Y	M	G	Q	F	Y	W
PDE1B	P	H	T	L	M	L	S	Q	F	I	N
PDE2	Q	T	A	I	Y	M	L	Q	F	M	W
PDE3	P	H	T	I	V	F	L	Q	F	I	W
PDE11	V	S	A	V	T	F	L	Q	W	I	W
PDE4	P	Y	T	I	M	M	S	Q	F	I	Y
PDE7	P	S	S	V	T	L	I	Q	F	M	W
PDE8	P	C	A	I	S	V	S	Q	F	I	W
PDE5	I	Q	A	V	A	M	M	Q	F	I	W
PDE6	I	Q	A	V	A	M	L	Q	F	I	W
PDE9	E	A	V	L	L	F	A	Q	F	I	Y

substrates. For PDE families with dual substrate specificity, the side chain of the invariant glutamine would freely rotate to form two hydrogen bonds with cAMP or cGMP.

The glutamine switch mechanism is supported by the structure of dual cAMP/cGMP-specific PDE1B (31), in which the glutamine is unbonded and could be freely rotated. However, it was challenged by two lines of evidence. First, the Q817A mutation of PDE5 weakened K_m for cGMP by 60-fold but did not significantly change K_m for cAMP (35). Second, the structure of dual-specific PDE2A3 shows that the side chain of Gln^{859} is fixed by a hydrogen bond with Tyr^{827} (22). Thus, for the glutamine to switch, this preexisting hydrogen bond has to be broken, and the net gain of energy will be zero.

The glutamine switch is even less likely in view of our PDE10A2 structure, in which the side chain of Gln^{726} is locked by two hydrogen bonds with Tyr^{693} and a water bound to Tyr^{730} and Trp^{762} (Fig. 2). In addition, two hydrogen bonds between Gln^{726} and N6 and N7 of cAMP in the PDE10A2 structure are in a totally different pattern from the bidentate bonds of N1 and N6 of the model cAMP predicted by the glutamine switch (31). The single contact between Gln^{726} and N7 of cGMP (Fig. 2) differs entirely from the two predicted hydrogen bonds between the glutamine and N1 and O6 of cGMP (31). Most importantly, different conformations and interactions between the products and the substrates suggest that the products are not a reasonable model for the substrate binding, at least in PDE10, although it is unknown how similar they are in other PDE families.

The present PDE10A2 structures reveal that cAMP and cGMP bind to the same pocket but have different orientations and interactions, suggesting that the substrate specificity is determined by a different binding of the substrates in the PDE10 family. The structure-based sequence alignment of the nucleoside-binding pocket, that we tentatively term "substrate specificity pocket" or S-pocket, shows dramatic variation of amino acids across PDE families (Table 2 and Fig. 4). Apparently, the amino acid variation not only represents changes of the chemical groups in the PDE families but also defines the shape and size of the binding pocket. To match the chemical nature and shape of the pocket, substrates may bind to individual PDE families in the same or different orientations and configurations with different affinity. In some extreme cases, poor substrate binding, such as K_m = 3.9 mM for cGMP in PDE7 (33) and $K_m > 100$ μM for cAMP in PDE9 (2), would explain their preferred cAMP or cGMP specificity. The invariant glutamine in the S-pocket provides hydrogen bonds for binding of substrates but may not be a key element in distinguishing substrates. Instead, multiple elements at the S-pocket must work together to determine the substrate specificity. Each amino acid in the S-pocket may contribute to the specificity differently but should not exclusively dominate the substrate specificity.

Methods

Protein Expression and Purification of PDE10A2. The cDNA of the catalytic domain of human PDE10A2 (GenBank BAA84467) was purchased from American Type Culture Collection (Manassas, VA). The coding region for amino acids 449–789 of PDE10A2 was amplified by PCR and subcloned into the expression vector pET15b. The resultant plasmid pET-PDE10 was transferred into *Escherichia coli* strain BL21 (CodonPlus) for overexpression. The *E. coli* cell carrying pET-PDE10 was grown in 2× YT medium at 37°C to absorption A_{600} = 0.7, and then 0.1 mM isopropyl β-D-

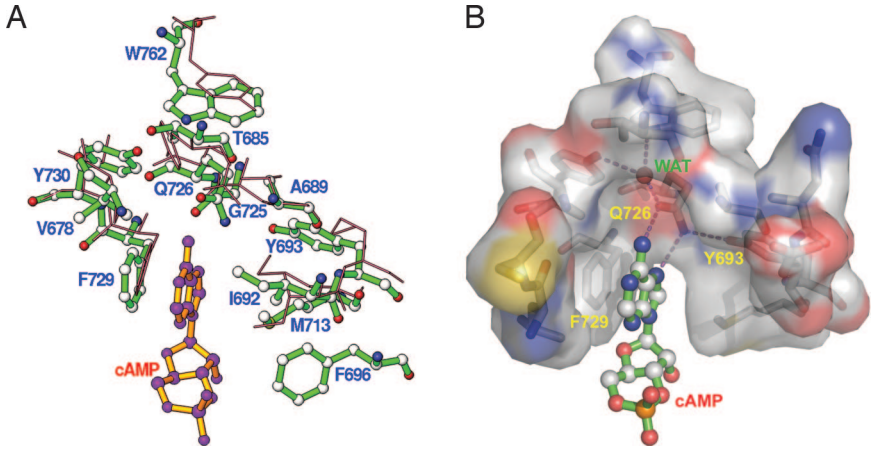

Fig. 4. A potential S-pocket. (*A*) The PDE10A2 residues (green bonds) are superimposed over the PDE4D2 residues (thinner salmon sticks). (*B*) Surface presentation of the S-pocket in PDE10.

thiogalactopyranoside was added for further growth at 20°C overnight. The recombinant PDE10 protein was purified on columns of nickel-nitrilotriacetic acid (Qiagen, Valencia, CA), Q-Sepharose, and Sephacryl S300 (Amersham Biosciences, Piscataway, NJ). A typical purification yielded ≈10 mg of PDE10A2 with a purity >95% from a 2-liter cell culture. The D674A and D564N mutants were produced by a QuikChange site-directed mutagenesis kit (Stratagene, La Jolla, CA) and verified by DNA sequencing. Overexpression and purification of the mutants used the same protocols for the wild-type protein.

Enzymatic Assay. Enzymatic activity of the catalytic domains of PDE10A2 and its mutants was assayed by using [^{3}H]cAMP or [^{3}H]cGMP (20,000 cpm per assay) as substrates in a reaction mixture of 20 mM Tris·HCl, pH 7.5/1.0 mM DTT/10 mM $MgCl_2$ at room temperature for 15 min (33). The reaction was terminated by the addition of 0.2 M $ZnSO_4$/$Ba(OH)_2$. Radioactivity of unreacted [^{3}H]cAMP or [^{3}H]cGMP in the supernatant was measured by a liquid scintillation counter. The turnover rate was measured at nine concentrations of substrate and at hydrolysis of 15–50% substrate. Each measurement was repeated three times. The parameters of K_m, k_{cat}, and V_{max} were calculated following steady-state kinetics.

Crystallization and Structure Determination. All crystals were grown by hanging drop and have the space group $P2_12_12_1$ with similar cell dimensions (Table 1). The unliganded PDE10A2 (449–789) was crystallized against a well buffer of 0.1 M Hepes, pH 7.5/0.2 M $MgCl_2$/50 mM 2-mercaptoethanol (2-ME)/16% PEG 3350. Crystals of the D564N and D674A mutants were grown against a well buffer of 0.1 M Hepes, pH 7.5/0.1 M $MgCl_2$/100 mM 2-ME/13% PEG 3350. The complexes of PDE10A2-AMP, PDE10A2-AMP, D674A-cAMP, D674A-cGMP, and D564N-cAMP were prepared by soaking the unliganded crystals in 20 mM cAMP or 30 mM cGMP in a buffer of 16% PEG 8000/0.1 M Hepes, pH 7.5/0.1 M $MgCl_2$/60 mM 2-ME at 4°C for 1.5–6 h. The crystallization buffer plus 20% ethylene glycol or 15% PEG 400 was used as the cryosolvent. Diffraction data were collected on beamline X29 at Brookhaven National Laboratory and processed by program HKL (Table 1) (40).

The structure of the unliganded PDE10A2 was solved by the molecular replacement program AMoRe (41), using the PDE4D2 catalytic domain as the initial model. The rotation and translation searches yielded two solutions that are obviously distinct from background and have correlation coefficients of 11.2 and 10.4 and *R* factors of 0.538 and 0.539 for 4543 reflections between 4 and 8 Å resolution. When the two solutions were added together, the correlation coefficient and *R* factor were improved to 0.21 and 0.51. The electron density map was improved by the density modification package of CCP4. The atomic model was rebuilt by program O (42) and refined by program CNS (Table 1) (43). The refined catalytic domain of the unliganded PDE10A2 was used to solve other structures.

We thank beamline X29 at National Synchrotron Light Source for collection of diffraction data, Drs. Richard Wolfenden and Charles Carter for proofreading the manuscript, and Xiuyan Qin for assistance on cell culture and protein expression. This work was supported in part by National Institutes of Health Grant GM59791 (to H.K.).

1. Bender AT, Beavo JA (2006) *Pharmacol Rev* 58:488–520.
2. Mehats C, Andersen CB, Filopanti M, Jin SL, Conti M (2002) *Trends Endocrinol Metab* 13:29–35.
3. Truss MC, Stief CG, Uckert S, Becker AJ, Wafer J, Schultheiss D, Jonas U (2001) *World J Urol* 19:344–350.
4. Liu Y, Shakur Y, Yoshitake M, Kambayashi JJ (2001) *Cardiovasc Drug Rev* 19:369–386.
5. Corbin JD, Francis SH (2002) *Int J Clin Pract* 56:453–459.
6. Lipworth BJ (2005) *Lancet* 365:167–175.
7. Castro A, Jerez MJ, Gil C, Martinez A (2005) *Med Res Rev* 25:229–244.
8. Menniti FS, Faraci WS, Schmidt CJ (2006) *Nat Rev Drug Discov* 5:660–670.
9. Galie N, Ghofrani HA, Torbicki A, Barst RJ, Rubin LJ, Badesch D, Fleming T, Parpia T, Burgess G, Branzi A, *et al*. (2005) *N Engl J Med* 353:2148–2157.
10. Soderling SH, Bayuga SJ, Beavo JA (1999) *Proc Natl Acad Sci USA* 96:7071–7076.
11. Fujishige K, Kotera J, Michibata H, Yuasa K, Takebayashi S, Okumura K, Omori K (1999) *J Biol Chem* 274:18438–18445.
12. Loughney K, Snyder PB, Uher L, Rosman GJ, Ferguson K, Florio VA (1999) *Gene* 234:109–117.
13. Seeger TF, Bartlett B, Coskran TM, Culp JS, James LC, Krull DL, Lanfear J, Ryan AM, Schmidt CJ, Strick CA, *et al*. (2003) *Brain Res* 985:113–126.
14. Kotera J, Sasaki T, Kobayashi T, Fujishige K, Yamashita Y, Omori K (2004) *J Biol Chem* 279:4366–4375.
15. Xie Z, Adamowicz WO, Eldred WD, Jakowski AB, Kleiman RJ, Morton DG, Stephenson DT, Strick CA, Williams RD, Menniti FS (2006) *Neuroscience* 139:597–607.
16. Coskran TM, Morton D, Menniti FS, Adamowicz WO, Kleiman RJ, Ryan AM, Strick CA, Schmidt CJ, Stephenson DT (2006) *J Histochem Cytochem* 54:1205–1213.
17. Hebb AL, Robertson HA, Denovan-Wright EM (2004) *Neuroscience* 123:967–981.
18. Hu H, McCaw EA, Hebb AL, Gomez GT, Denovan-Wright EM (2004) *Eur J Neurosci* 20:3351–3363.
19. Siuciak JA, McCarthy SA, Chapin DS, Fujiwara RA, James LC, Williams RD, Stock JL, McNeish JD, Strick CA, Menniti FS, Schmidt CJ (2006) *Neuropharmacology* 51:374–385.
20. Siuciak JA, Chapin DS, Harms JF, Lebel LA, McCarthy SA, Chambers L, Shrikhande A, Wong S, Menniti FS, Schmidt CJ (2006) *Neuropharmacology* 51:386–396.
21. Rodefer JS, Murphy ER, Baxter MG (2005) *Eur J Neurosci* 21:1070–1076.
22. Iffland A, Kohls D, Low S, Luan J, Zhang Y, Kothe M, Cao Q, Kamath AV, Ding YH, Ellenberger T (2005) *Biochemistry* 44:8312–8325.
23. Xu RX, Hassell AM, Vanderwall D, Lambert MH, Holmes WD, Luther MA, Rocque WJ, Milburn MV, Zhao Y, Ke H, Nolte RT (2000) *Science* 288:1822–1825.
24. Xu RX, Rocque WJ, Lambert MH, Vanderwall DE, Luther MA, Nolte RT (2004) *J Mol Biol* 337:355–365.
25. Sung BJ, Hwang KY, Jeon YH, Lee JI, Heo YS, Kim JH, Moon J, Yoon JM, Hyun YL, Kim E, *et al*. (2003) *Nature* 425:98–102.
26. Huai Q, Wang H, Sun Y, Kim HY, Liu Y, Ke H (2003) *Structure (London)* 11:865–873.
27. Huai Q, Colicelli J, Ke H (2003) *Biochemistry* 42:13220–13226.
28. Huai Q, Liu Y, Francis SH, Corbin JD, Ke H (2004) *J Biol Chem* 279:13095–13101.
29. Huai Q, Wang H, Zhang W, Colman R, Robinson H, Ke H (2004) *Proc Natl Acad Sci USA* 101:9624–9629.
30. Scapin G, Patel SB, Chung C, Varnerin JP, Edmondson SD, Mastracchio A, Parmee ER, Singh SB, Becker JW, Van der Ploeg LH, Tota MR (2004) *Biochemistry* 43:6091–6100.
31. Zhang KY, Card GL, Suzuki Y, Artis DR, Fong D, Gillette S, Hsieh D, Neiman J, West BL, Zhang C, *et al*. (2004) *Mol Cell* 15:279–286.
32. Card GL, England BP, Suzuki Y, Fong D, Powell B, Lee B, Luu C, Tabrizizad M, Gillette S, Ibrahim PN, *et al*. (2004) *Structure (London)* 12:2233–2247.
33. Wang H, Liu Y, Chen Y, Robinson H, Ke H (2005) *J Biol Chem* 280:30949–30955.
34. Wang H, Liu Y, Huai Q, Cai J, Zoraghi R, Francis SH, Corbin JD, Robinson H, Xin Z, Lin G, Ke H (2006) *J Biol Chem* 281:21469–21479.
35. Zoraghi R, Corbin JD, Francis SH (2006) *J Biol Chem* 281:5553–5558.
36. Yathindra N, Sunderalingam M (1974) *Biochem Biophys Res Commun* 56:119–126.
37. Butt E, Beltman J, Becker DE, Jensen GS, Rybalkin SD, Jastorff B, Beavo JA (1995) *Mol Pharmacol* 47:330–339.
38. Butt E, Beltman J, Becker DE, Jensen GS, Rybalkin SD, Jastorff B, Beavo JA (1995) *Mol Pharmacol* 47:340–347.
39. Lee CH, Evans FE, Sarma RH (1975) *J Biol Chem* 250:1290–1296.
40. Otwinowski Z, Minor W (1997) *Methods Enzymol* 276:307–326.
41. Navaza J, Saludjian P (1997) *Methods Enzymol* 276:581–594.
42. Jones TA, Zou J-Y, Cowan SW, Kjeldgaard M (1991) *Acta Crystallogr A* 47:110–119.
43. Brünger AT, Adams PD, Clore GM, DeLano WL, Gros P, Grosse-Kunstleve RW, Jiang JS, Kuszewski J, Nilges M, Pannu NS, *et al*. (1998) *Acta Crystallogr D* 54:905–921.